Navier-Stokes Study of Rotating Stall in Compressor Cascades

F. Davoudzadeh,* N.-S. Liu,† S. J. Shamroth,‡ and S. J. Thoren§
Scientific Research Associates, Inc., Glastonbury, Connecticut

Numerical simulations of unsteady flow in a linear cascade of J-79 stator blades are conducted with a finite-difference method. The flowfield is determined by solving two-dimensional compressible Navier-Stokes equations. The effects of turbulence are accounted for by a mixing length model. The initial condition consists of introducing localized finite disturbance into the heavily loaded cascade flow. Depending on the values of the inlet swirl angle, several different flow regimes are obtained, including stall propagation. The results correlate reasonably well with relevant experimental data for rotating stall inception and show the physical features of the process.

Introduction

THE phenomenon of rotating stall represents a potentially serious problem that must be recognized during the design and operation of a compression system. In rotating stall, a major separation region appears in one or more adjacent passages, and this separation zone then propagates circumferentially with time. As the zone propagates to an adjacent passage, the original passage "unstalls," and the process continues. Stall may appear as a single propagating cell or multiple propagating cells.

Rotating stall is associated with decreased compressor performance which, in itself, is a significant problem. Furthermore, the large unsteady effects associated with rotating stall can be a factor in blade fatigue and can be a precursor to destructive failure of the component. Therefore, analyses and experiments that shed further light on rotating stall phenomena represent important additions to the knowledge base.

Large-scale unsteady separation is a basic feature of the process. Because rotating stall is initiated from separated flow, viscous effects that lead to, and then control, separation are important. Three-dimensional effects may be important; in particular, part-span stall, in which a stall cell occurs over only a portion of the blade passage, and full-span stall are both observed. Finally, in actual operation, stall may be a multiblade row phenomenon in which the presence of additional blade rows significantly affects the observed flow pattern, with the interaction effect dependent on blade row spacing.

Most previous efforts have approached the problem via linearized inviscid equations, with the blade row represented by an actuator disk (e.g., Refs. 1-8), approaches based on component modeling (e.g., Refs. 9-15), and approaches based on vortex method simulation (e.g., Refs. 16 and 17).

Whereas the works of Refs. 1-8 and other work of this type demonstrate some of the important features of rotating stall, the common approach is an inviscid one with empirical cascade turning and loss characteristics. Although inviscid flow is a reasonable assumption upstream of the blade row, it is not downstream of the blade row, where nonuniform flows associated with wakes and stall cells are important. A second drawback of this approach is the use of an empirical cascade model. It is in the blade passage region that the stall process is initiated, and use of an actuator disk model here requires a specific data base. Furthermore, these approaches do not consider the basic process within the cascade and, therefore, do not give clear guidance as to how the rotating stall process may be suppressed.

The vortex method approach of Refs. 16 and 17 does not require cascade loss and turning data, but it, too, has limitations. As applied in Refs. 16 and 17, the flow is represented by a large collection of discrete vortices, whose motions are tracked in time by an algorithm based on the two-dimensional, incompressible Euler equations. The near-wall effects of viscosity are accounted for by the creation of discrete vortex sheets consistent with the no-slip condition. A semiempirical boundary-layer routine is used to estimate the locations of the separation points, and boundary vortices are released into the flow downstream of the separation points. It is noted here that, in many cases of practical interest, much, if not all, of the cascade passage contains viscous effects and the flow is compressible. Furthermore, it is not clear how to extend the vortex method to treat three-dimensional simulations.

The present effort applies a two-dimensional, unsteady Navier-Stokes analysis to the rotating stall problem. Before discussing the work in detail, it is useful to discuss both the potential and the limitations of such an analysis. Regarding first the limitations, it is clear that a two-dimensional simulation does not contain all of the relevant flow physics. A variety of experiments indicate the presence of strong radial flows when a stall cell is present; a two-dimensional analysis cannot model these three-dimensional effects. A second major limitation of a Navier-Stokes procedure is that of turbulence modeling. Appropriate turbulence modeling for highly three-dimensional unsteady flows, such as those found in a fully developed rotating stall cell, is still a significant problem. Although two-dimensional and turbulence model assumptions, along with grid resolution questions, still must be addressed, the present Navier-Stokes approach represents an initiation of a basic study of this very complex problem. It can include inlet distortion and large-amplitude disturbance effects[18] and has the potential for extension to three dimensions.

In this paper, studies will focus on the stall inception portion of the overall rotating stall problems. The inception of rotating stall represents a limit to the useful operation of aircraft gas turbine engines. Considerable effort has been

Presented as Paper 88-3265 at the AIAA/ASME/SAE/ASEE 24th Joint Propulsion Conference, Boston, MA, July 12-13, 1988; received July 18, 1988; revision received May 31, 1989.

*Research Scientist.
†Senior Research Scientist; currently at NASA Lewis Research Center, Cleveland, OH. Member AIAA.
‡Vice President. Member AIAA.
§Associate Research Scientist.

expended to investigate this problem. Nevertheless, insufficient attention has been paid to the various instability mechanisms leading to stall propagation and the unsteady responses of the blade flow in the near-stall regime. Several flow instability initiation mechanisms can lead to rotating stall, such as inlet and exit flow distortions, flow separations in one of the blade passages due to extrinsic excitation, and rotor transients. As a first attempt, the present effort uses localized wall transpiration to trigger flow instabilities that might lead to stall propagation in a five-passage cascade. These results demonstrate the ability of the present Navier-Stokes procedure to simulate the flow processes associated with the rotating stall phenomenon. Thus, a framework is provided for examining the essential fluid dynamics associated with rotating stall inception.

Governing Equations and Solution Algorithm

The equations used are the ensemble-averaged, time-dependent Navier-Stokes equations, which can be written in vector form as

Continuity:

$$\frac{\partial \rho}{\partial t} + \nabla \cdot \rho \boldsymbol{U} = 0 \tag{1}$$

Momentum:

$$\frac{\partial \rho \boldsymbol{U}}{\partial t} + \nabla \cdot (\rho \boldsymbol{U}\boldsymbol{U}) = -\nabla P + \nabla \cdot (\bar{\bar{\pi}} + \bar{\bar{\pi}}^T) \tag{2}$$

Energy:

$$\frac{\partial \rho h}{\partial t} + \nabla \cdot (\rho \boldsymbol{U} h) = -\nabla \cdot (\boldsymbol{Q} + \boldsymbol{Q}^T) + \frac{\mathrm{D}P}{\mathrm{D}t} + \Phi + \rho\epsilon \tag{3}$$

where ρ is density, $\boldsymbol{U}$ velocity, P pressure, $\bar{\bar{\pi}}$ the molecular stress tensor, $\bar{\bar{\pi}}^T$ the turbulent stress tensor, h enthalpy, $\boldsymbol{Q}$ the mean heat flux vector, $\boldsymbol{Q}^T$ the turbulent heat flux vector, Φ the mean flow dissipation rate, and ϵ the turbulence energy dissipation rate. If the flow is assumed to have a constant total temperature, the energy equation is replaced by

$$T_t = T + \frac{q^2}{2C_p} = \text{const} \tag{4}$$

where T_t is the total temperature, q the magnitude of the velocity, and C_p the specific heat at constant pressure. In this work, the total temperature has been assumed constant to reduce computer run time.

In regard to the numerical method, the basic method used is that of Briley and McDonald, which is a linearized block implicit alternating direction implicit procedure. Further details of this procedure can be found in Refs. 19 and 20. As for the boundary conditions, total pressure, total temperature, and inlet swirl angle are specified along the inlet of the cascade. Along the exit of the cascade, only the static pressure is prescribed. On the blade surfaces, no-slip conditions are used for velocity components, whereas the pressure gradient normal to the wall is assumed to be zero. Finally, along the top and bottom boundaries of the cascade, periodic conditions are applied. These boundary conditions are chosen so as to be compatible with a characteristic analysis of the inviscid flow equations, and a full discussion is presented in Refs. 21 and 22.

Although the authors recognize that turbulence modeling for complex flows remains an important issue, the present effort uses a simple mixing length model. Whereas a more general model, such as a k-ϵ model, might be advantageous, particularly when large regions of separated flow are present, the mixing length approach should suffice in the present work, which seeks to demonstrate the applicability of a finite-difference Navier-Stokes approach to this problem. A more sophisticated turbulence model could be incorporated in the procedure in future efforts. The model is divided into wall and wake regions. In both regions, the turbulent viscosity is related to the mean flowfield via

$$\mu_T = \rho \ell^2 \left[\left(\frac{\partial u_i}{\partial x_j} + \frac{\partial u_j}{\partial x_i} \right) \frac{\partial u_i}{\partial x_j} \right]^{1/2} \tag{5}$$

where μ_T is the turbulent viscosity, ρ the density, ℓ the mixing length, u_i the ith velocity component, and x_i the ith Cartesian direction. Summation is implied for the repeated indices. The question now arises as to specification of ℓ. For the region upstream of the trailing edge, the mixing length is specified in the usual boundary-layer manner.[21,22] The region downstream of the blade trailing edge follows the model of Rudy and Bushnell.[23]

The final item to be considered is numerical or artificial dissipation. To the authors' best knowledge, all Navier-Stokes numerical analyses that are applied to the high Reynolds number problems typical of turbomachinery application require some artificial dissipation to suppress nonphysical spatial oscillations. The approach used in the present effort is based on the use of the second-order anisotropic artificial dissipation term. Details of this approach are given in Refs. 21 and 22.

Experimental Background

The blade considered is that of the stator set no. 1 described in Ref. 24. This stator set has been the subject of extensive experimental investigation. Briefly, stator set no. 1 is a shortened-span modification to the original fifth-stage stator row of the J-79 compressor. It contains 54 blades, and the resulting solidity ratio at midannulus is 0.85. The stator set is tested downstream of a guide vane row, which is used to vary the inlet swirl at a fixed stator stagger angle. The inlet swirl is increased until rotating stall is observed on the stator row. Rotating stall is detected through the use of quarter-chord pressure taps at mid-annulus on the suction surface of the stator blades. The complete set of experimental observations and the rotating stall inception boundaries can be found in Ref. 24. Two types of rotating stall inception have been detected; for most stagger angles tested, the so-called "small-amplitude inception" has been observed. In this case, the detectors indicate a relatively clean flow over the blades prior to rotating stall inception. Rotating stall begins intermittently with relatively small amplitude and then becomes steady after a small increase in the inlet swirl. At 40-deg mid annulus stagger angle, the stall inception boundary in terms of the overall inlet swirl angle is somewhere between 58 and 59 deg. The overall inlet swirl angle is obtained by integrating the circumferentially averaged swirl angle distributions along a radius.

Cascade Characteristics and Simulation Conditions

The numerical simulations are conducted for a two-dimensional linear cascade. The blade shape is the same as the midspan section of stator set no. 1. The stagger angle is 40 deg, and the solidity is 0.85. These values are made to be those of stator set no. 1 at the mid-annulus. The grid used in both the single- and multiple-passage calculations is shown in Fig. 1. This is a modified C-type grid with 149×35 grid points per passage. The inlet swirl angle β used in the present simulations is also defined in Fig. 1, and it corresponds to the overall inlet swirl in the experiments described in the previous section.

The Reynolds numbers of the present calculations are approximately 0.6×10^5, which are very close to those tested in Ref. 24. It is noted here that the Reynolds number is based on the axial cord length and the velocity magnitude at the inlet. The tests of Ref. 24 were run at inlet Mach numbers of approximately 0.1. In the present effort, calculations are carried out at higher inlet Mach numbers, 0.4, to avoid the very small time steps required because of the stiffness of the equations at low Mach numbers. It is expected that the compress-

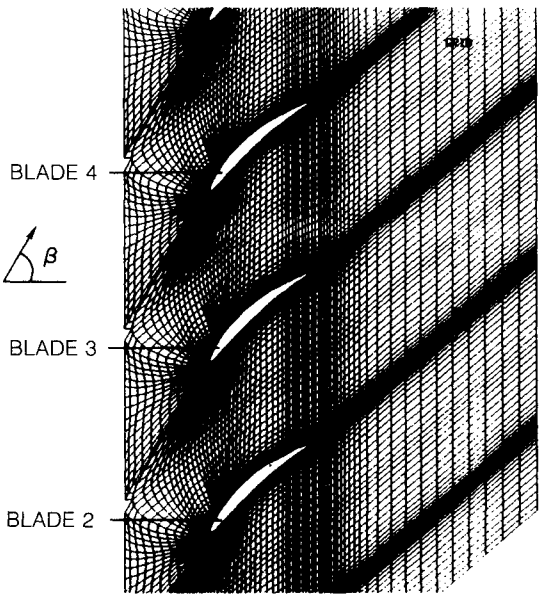

Fig. 1 Grid distribution.

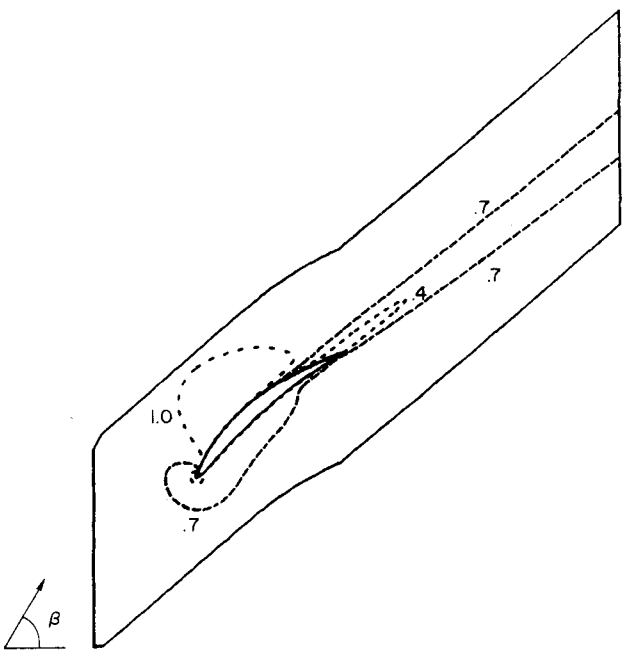

Fig. 2 Contour of axial velocity at $\beta = 57.0$ deg.

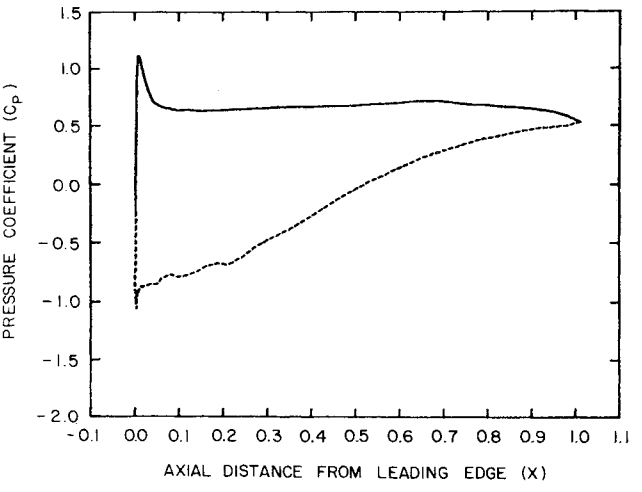

Fig. 3 Surface pressure distribution $\beta = 57.0$ deg.

ibility effects are of minor physical importance at this Mach number.

The work discussed here consisted of three types of calculations. First, single-passage flows were investigated, and the limit of inlet swirl angle for which a steady flow could be obtained was determined. These flows were then subjected to an extrinsically excited disturbance, and their response to these disturbances was determined. Finally, multiple-passage configurations subjected to extrinsically excited disturbances were considered. The aim of the last set of calculations was to determine the conditions under which a temporarily applied disturbance could lead to a self-sustaining propagating stall cell.

Single-Passage Flows in Near-Stall Regime

Five different cases are carried out for a single-passage cascade: 1) $\beta = 57$ deg, 2) $\beta = 58.5$ deg, 3) $\beta = 59$ deg, 4) $\beta = 60$ deg, and 5) $\beta = 61$ deg, where β is the swirl angle of the incoming flow. The purpose of these simulations is to assess the qualitative consistency between the numerical results and the relevant experimental results insofar as the inception of unsteady stall is concerned. These calculations were carried out under the condition of single blade periodicity.

The contours of axial velocity and the surface pressure distribution, for $\beta = 57.0$ deg, are shown in Figs. 2 and 3, respectively. As the inlet swirl angle increases, a small recirculation region starts to develop on the suction side of the trailing edge. In addition, the size of the wake also increases with increasing β. For cases 1–4, the simulations all reach an asymptotic steady state. However, in $\beta = 61$ deg, an asymptotic steady state cannot be established; in fact, the calculated flow exhibits significant unsteadiness, as indicated in Fig. 4. The recirculation region is enclosed by the zero-value contour line (a solid line) in axial velocity contour plots. An increment, $\Delta t = 1.0$, is the time required for a particle at freestream velocity to traverse one axial chord. At some instant, $t = t_0$, there is a large separation zone attached to the suction side of the trailing-edge region. Subsequently, it breaks away from the trailing edge so that a relatively smaller separation region still attaches to the trailing edge while a free recirculating zone of significant size appears in the near-wake region, as shown in Fig. 4b for $t - t_0 = 14.33$. This is further illustrated in Fig. 5, which is a velocity-vector field. Two recirculation zones are clearly discernible. This set of simulations indicates that, for single-passage flows, the inception boundary of unsteady stall is approximately at $\beta = 60$ deg. It is of interest to note that this unsteady stall inception boundary for single-passage flow is close to the rotating stall inception boundary for multiple-passage flow given by the most relevant experimental results, as briefly described in the "Experimental Background" section.

Single-Passage Flows Subject to Extrinsic Disturbances

There are several flow instability initiation mechanisms that can lead to rotating stall, such as inlet and exit flow distortions, flow separation in one of the blade passages due to extrinsic excitation, and rotor transients. The present approach seeks to introduce a temporary disturbance that most directly affects the passage flowfield and then removes the disturbance and determines whether the flow relaxes to its original state or a self-sustaining disturbance has been created. Although any of the aforementioned disturbances could be considered, interest in minimizing computer run time argues for a disturbance that directly affects the passage flow; there-

fore, wall transpiration over the aft 50% of the suction surface was chosen.

Before the disturbance for a multiple-passage calculation was introduced, the effect of wall transpiration disturbance on a single-passage flowfield was considered. Two series of unsteady calculations are performed for single-passage cascade flows. In the first series of calculations, the baseline flow is the steady-state solution for $\beta = 57$ deg. In the second series of calculations, the baseline flow is the steady-state solution for $\beta = 60$ deg. Both of these have been described in the preceding section. At some instant (i.e., $t = 0$), a disturbance is applied to these baseline flows through the injection toward the upstream direction. The strength of the jet is approximately 5% of the inlet velocity, and the spatial extent of the injection is about 50% of the axial chord.

For $\beta = 57$ deg, the introduction of a wall jet leads to a change in the flowfield; however, a new steady state is reached by $t = 8.0$. For $\beta = 60$ deg, in contrast to the 57-deg case, introduction of the wall jet leads to a solution that exhibits periodic shedding and does not reach an asymptotic steady state. More specifically, after the disturbance is in effect for 4.0 nondimensional time units, a large separation zone develops. Subsequently, the large separation zone splits into two or more recirculation zones moving downstream. This process then repeats itself. At $t = 24.0$, the disturbance is then removed, and the flow eventually returns to its initial flowfield, implying the uniqueness of the solution. These results suggest that the present solution is numerically stable over the range of β of interest and that unsteadiness exhibited in the disturbed flow can be viewed as physically meaningful.

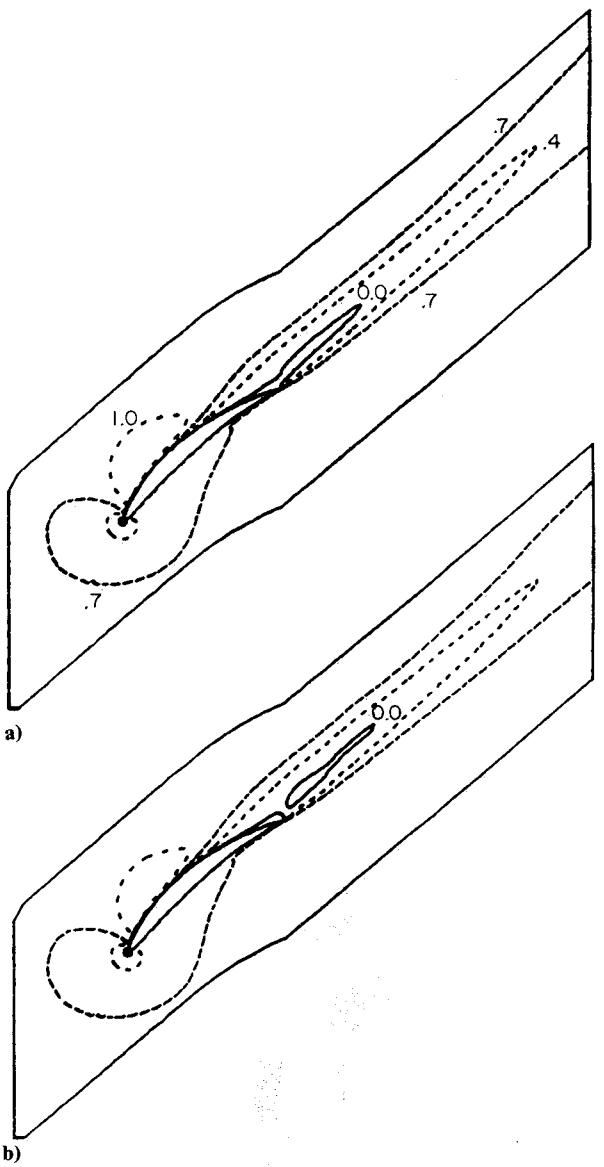

Fig. 4 Contour of axial velocity: a) $\beta = 61.0$ deg, $t = t_0$; b) $\beta = 61.0$ deg, $t = t_0 + 14.33$.

Multiple-Passage Calculations

The final set of calculations conducted are for a five-passage configuration. The most relevant experimental investigation and the results have been briefly discussed in previous sections.

The calculations are performed at various inlet swirl angles by first obtaining an asymptotic steady solution at that angle. A wall jet disturbance is then introduced on the suction surface of the second blade (see Fig. 1) in the manner described earlier. Typically, a stall zone appears that may or may not propagate. After some time, the disturbance is removed and the unsteady responses of the flow followed. Details of these cases can be found in Ref. 18.

Case 1: $\beta = 57$ Deg

Following the introduction of the disturbance to the baseline flow for eight time units, a new steady solution is obtained. however, this new flowfield is not periodic on a passage-by-passage basis. Furthermore, although the extrinsic disturbance is applied on the second blade, changes are also noted on both the first and third blade flowfields. Specifically, a distinct and observable separation zone appears in the aft region of the second blade suction surface, while the leading-edge regions of both the first and third blades are also affected. The effective incidence on the first passage has been decreased, and that on the third has been increased. This is consistent with the usual explanation of the rotating stall process occurring as a result of blockage effects. According to this theory (e.g., Ref. 1), if the flow condition is such that the cascade is heavily loaded, this increase in incidence of the third passage tends to stall the third passage. A stalled third passage then tends to relieve the second passage stall and, therefore, after some time period, the stall zone originally observed on the second blade proceeds to the third blade. Although this basic mechanism of changed incidence angles is observed in this calculation, no propagation is observed under this particular inlet swirl condition, and rather a new steady flow pattern has been attained.

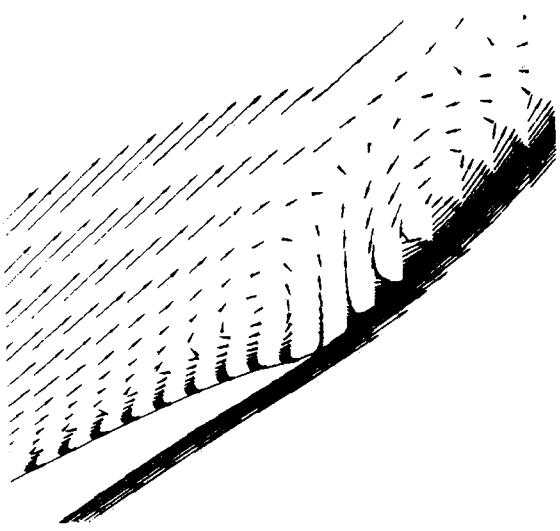

Fig. 5 Velocity vector field at trailing edge: $\beta = 61.0$ deg, $t - t_0 = 14.33$.

Table 1 Blade flow properties for 61-deg case; X indicates large separation zone; 0 indicates small separation zone

	Blade no.				
t	1	2	3	4	5
12	0	0	0	X	X
16	X	0	0	X	X
20	X	X	0	0	0
24	X	X	X	0	0
28	0	0	X	X	0
32	0	0	X	X	0
36	0	0	0	X	X

Case 2: β = 61 Deg

As in the case of the single-passage 61-deg calculation, the baseline flow contains separation zones in each passage. At t = 4.0, a disturbance is introduced on the second blade; this is maintained until t = 8.0, when it is removed.

Table 1 presents the developing pattern between t = 12 and t = 36. As can be seen, the large separation region propagates in the direction from blades 1 to 5. It is clear that each passage at all times contains separated flow and that, although the region of most intense flow separation does propagate, passages do not fully recover. This is not the usual behavior associated with "small-amplitude" rotating stall.

Case 3: β = 60 Deg

At this angle, no significant separation zone exists in the absence of external disturbance. Upon introduction of the wall disturbance, a significant separation zone appears and, in this case, propagates toward blade 3. The wall disturbance is maintained until the separation zone reaches blade 3, with some effect noted on blade 4. The disturbance is then removed and, although some propagation continued, the separation zones rapidly shrink and eventually disappear.

Case 4a: β = 60.5 Deg

Three separate cases are run at 60.5-deg inlet swirl angle. All cases are initiated from the same baseline solution (Fig. 6a); the difference is the introduction, maintenance, and reinforcement of extrinsic disturbances. The time step used in these calculations is kept at a constant value of 0.02.

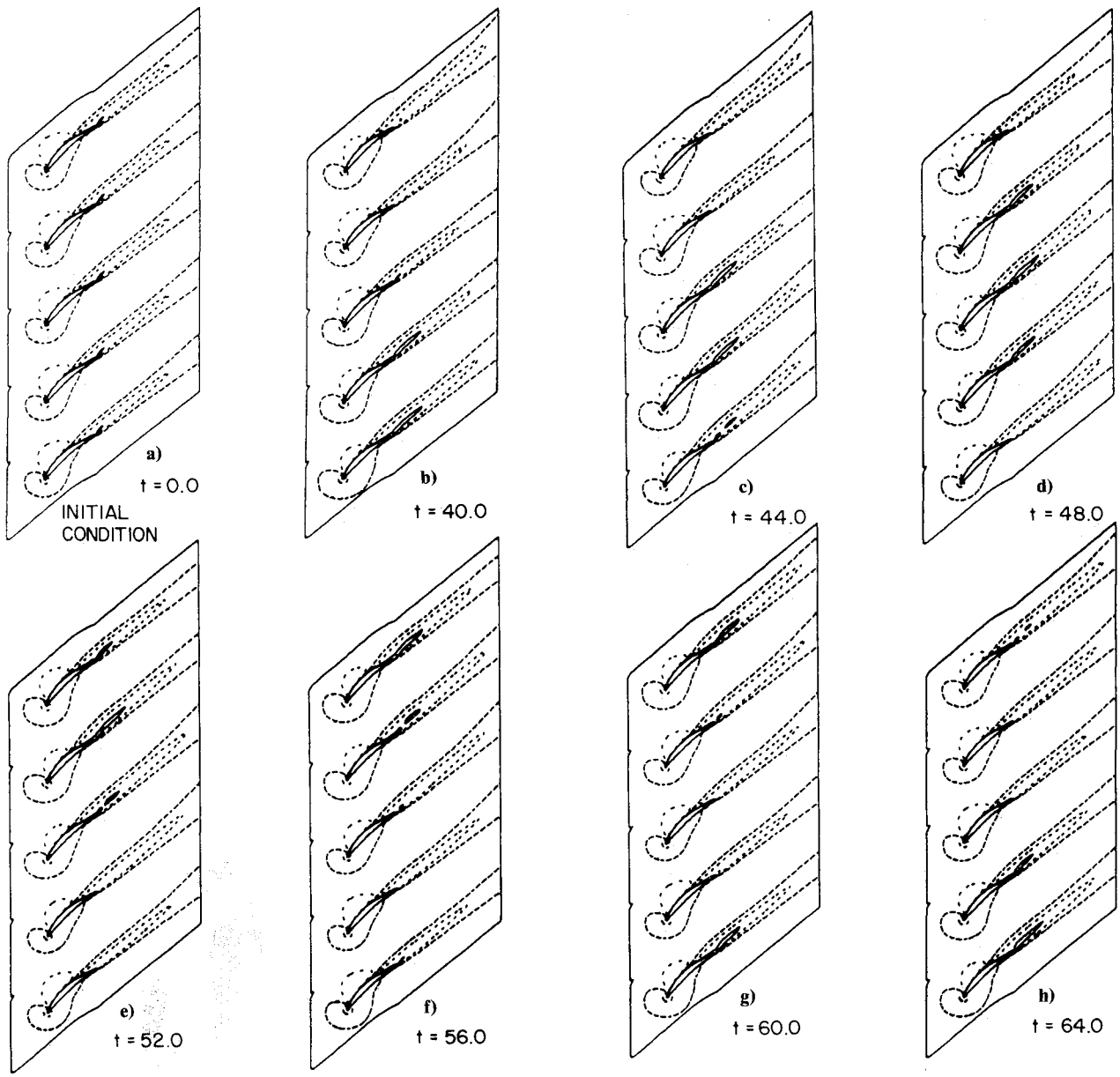

Fig. 6 Streamwise velocity contours during one complete cycle of the stall propagation (β = 60.5, at t = 32.0, all extrinsic disturbances removed).

The case 4a calculation is initiated by introducing a disturbance in the second passage. This wall transpiration disturbance is held until $t = 24$, when it is removed. The calculation is then allowed to proceed. Although the subsequent flow evolution does show a propagation of undiminished separation zone(s) from passage to passage, the propagating pattern is not regular; i.e., this way of introducing disturbance does not lead to a clear rotating stall pattern. In order to ascertain the dependence of the developed flow on the ways of introducing disturbances and, later, reinforcing the numerically diffused propagation, the following two cases are investigated.

Case 4b: $\beta = 60.5$ Deg

In this case, a disturbance in the form of wall transpiration is imposed on a segment of the suction surface of the second blade until $t = 24.0$. At this time, some stall propagation has been developed; i.e., a relatively weak, yet still appreciable, recirculation region emerges on the fourth blade. In order to compensate for the effects of numerical diffusion on the inception of stall propagation, this weak recirculation zone is then strengthened by introducing a wall transpiration on the fourth blade and, at the same time, the wall blowing at the second blade is removed. Finally, the fourth blade disturbance is also removed at $t = 32.0$, and the subsequent evolution of such a disturbed flow is examined. The results presented in Figs. 6b–6h demonstrate the rotation of the stall cell through one complete cycle. The stall cell is indicated by the region enclosed by solid contour lines of streamwise velocity. This calculation has been continued for three cycles, and the propagating speed of the cell is approximately 0.23 times the undisturbed upstream transverse velocity.

Case 4c: $\beta = 60.5$ Deg

This case is a continuation of the study of the dependence of the resulting pattern on the manner in which disturbances are reinforced. In this calculation, the disturbance is reinforced by continuing the wall blowing on blade 2 while adding wall blowing on blades 3 and 4. After a period of time, the wall blowings are then removed. The results are very similar to those of case 4b, and so these results will not be shown here. The results of case 4b and 4c suggest that very similar rotating stall patterns could be triggered by quite different initial disturbances, thus indicating a lack of sensitivity to the details of the disturbance.

Summary and Concluding Remarks

A summary of the five-passage calculations is given in Table 2. The results at 57 deg showed that introduction of a disturbance gave significant change in the passage-to-passage flow but that no propagation of the disturbance from passage to passage was noted. At 60 deg, introduction of a disturbance again led to a loss of passage-to-passage periodicity and development of a flow separation region. Although this region did propagate in the passage-to-passage direction, once the disturbance was removed, the flow returned to its original state; the propagation triggered by the disturbance was not self-sustaining.

The 60.5-deg case showed a markedly different behavior. Three different ways of introducing/reinforcing disturbances were investigated, and all showed undiminished propagation after their removal. Two of them eventually led to clear patterns of rotating stall. This would associate $\beta = 60.5$ deg with the inception of rotating stall for five-passage cascade. This correlates well with the inception boundary noted experimentally in Ref. 24.

In regard to the flow physics, the calculations appear to confirm that the propagation mechanism is a change in effective incidence resulting from blockage. In all of the previously discussed numerical simulations, the time history of the static pressure at the quarter-chord point on the suction side of each blade has been stored. A comparison between these pressure-time records and the corresponding flow patterns in terms of the velocity contours, such as Fig. 6, indicates that the blade immediately prior to the onset of propagating stall at first experiences an increase in the static pressure. Subsequently, such an increased pressure is associated with the stall of this blade. Later, when the stalled region starts to shrink, this pressure also begins to decrease, until the stalled region is propagated to the next blade. A typical pressure-time variation during the onset-development-decay cycle of the stalled region is illustrated in Fig. 7. It is noted here that the variation of the pressure in the leading-edge region is directly related to the change of incidence angle. Figure 8 compares surface pressure on blades 1 and 3 at an instant corresponding to the state indicated by Fig. 6b; the decreased loading on stalled blades is obvious.

The stall cells of the present simulation are significant but do not dominate the entire passage. This is consistent with the fact that they are associated with the so-called small-amplitude rotating stall inception. Although certain approximations in regard to two-dimensional flow, turbulence modeling, etc., are obviously present, the results correlate well with the most relevant data for rotating stall inception and show the physical features of the process.

Table 2 Summary of five-passage cascade calculations

Inlet swirl angle, deg	Observed
57	Steady flow with injection on; return to original state when injection removed
60	Limited stall propagation with injection on; return to original state when injection removed
60.5	Stall propagation with injection on; cyclic stall propagation established after injection removed
61	Separation in all passages with/without injection; propagation pattern dissimilar to that of rotating stall

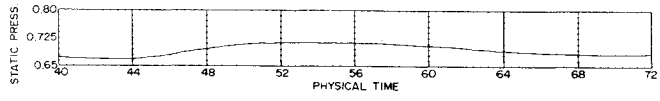

Fig. 7 Typical pressure variation at the quarter-chord suction side point during the onset-development-decay cycle of the stalled region.

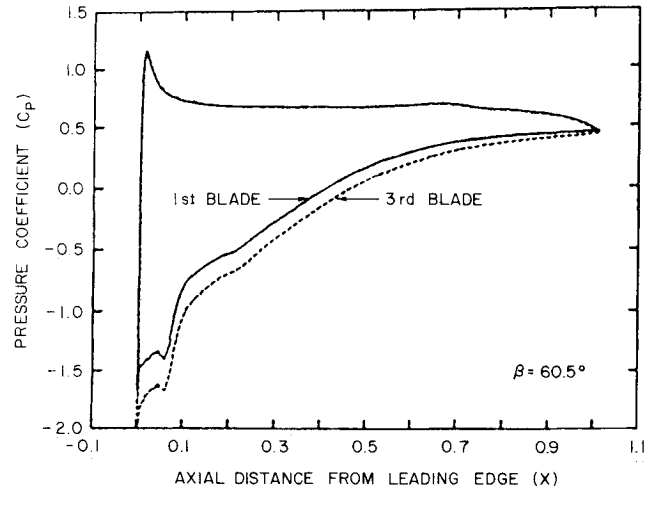

Fig. 8 Surface pressure distribution on blades stalled (first blade) and unstalled regions (third blade) of the five-passage cascade.

Acknowledgments

This work was sponsored by the Air Force Wright Aeronautical Laboratories under Contract F33615-84-C-2479. The authors gratefully acknowledge the assistance of Lt. Scott Richardson of AFWAL and Richard C. Buggeln of Scientific Research Associates, Inc., during the course of this effort. We are also thankful to L. Smith and M. Suo of General Electric for furnishing the blade coordinates information.

References

[1]Marble, F. E., "Propagation of Stall in a Compressor Blade Row," *Journal of the Aeronautical Sciences,* Vol. 22, 1955, pp. 541–554.

[2]Emmons, H. W., Kronauer, R. E., and Rockett, J. A., "A Survey of Stall Propagation—Experiment and Theory," *Journal of Basic Engineering,* Vol. 81, 1959, pp. 409–416.

[3]Takata, H. and Nagano, S., "Nonlinear Analysis of Rotating Stall," *Journal of Engineering for Power,* Vol. 84, 1972, pp. 279–293.

[4]Adamczyk, J. J., "Unsteady Fluid Dynamic Response of an Isolated Rotor with Distorted Inflow," AIAA Paper 74-49, Jan. 1974.

[5]Nenni, J. P. and Ludwig, G. R., "A Theory to Predict the Inception of Rotating Stall in Axial Flow Compressors," AIAA Paper 74-528, 1974.

[6]Ludwig, G. D., Nenni, J. P., and Erickson, J. C., Jr., "Investigation of Rotating Stall Phenomena in Axial Flow Compressors, Vol. I—Basic Studies of Rotating Stall," AFAPL-TR-76-48, June 1976.

[7]Ludwig, G. R., and Nenni, J. P., "Basic Studies of Rotating Stall in Axial Flow Compressors," AFAPL-TR-79-2083, Sept. 1979.

[8]Nenni, J. P., Homicz, G. F., and Ludwig, G. R., "Rotating Stall Investigations, Vol. I—Theoretical Investigations," AFWAL-TR-83-2002, 1983.

[9]Greitzer, E. M., "Review—Axial Compressor Stall Phenomena," *Journal of Fluids Engineering,* Vol. 102, 1980, pp. 134–151.

[10]Greitzer, E. M., "The Stability of Pumping Systems," *Journal of Fluids Engineering,* Vol. 103, 1981, pp. 193–242.

[11]Cumpsty, N. A. and Greitzer, E. M., "A Simple Model for Compressor Stall Propagation," *Journal of Engineering for Power,* Vol. 104, 1982, pp. 170–176.

[12]Moore, F. K., "A Theory of Rotating Stall of Multistage Axial Compressors: Part I—Small Disturbances," *Journal of Engineering for Gas Turbines and Power,* Vol. 106, 1984, pp. 313–320.

[13]Moore, F. K., "A Theory of Rotating Stall of Multistage Axial Compressors: Part II—Finite Disturbances," *Journal of Engineering for Gas Turbines and Power,* Vol. 106, 1984, pp. 321–336.

[14]Moore, F. K. and Greitzer, E. M., "A Theory of Post-Stall Transients in Axial Compressor Systems: Part I—Development of Equations," *Journal of Engineering for Gas Turbines and Power,* Vol. 108, No. 1, 1986, pp. 68–76.

[15]Moore, F. K. and Greitzer, E. M., "A Theory of Post-Stall Transients in Axial Compressor Systems: Part II—Application," *Journal of Engineering for Gas Turbines and Power,* Vol. 108, 1986, pp. 231–239.

[16]Spalart, P. R., "Two Recent Extensions of the Vortex Method," AIAA Paper 84-0343, 1984.

[17]Speziale, C. G., Sisto, F., and Jonnavithula, S., "Vortex Simulation of Propagating Stall in a Linear Cascade of Airfoils," *Journal of Fluids Engineering,* Vol. 108, 1986, pp. 304–312.

[18]Davoudzadeh, F., Liu, N.-S., Shamroth, S. J., and Thoren, S. J., "A Navier-Stokes Study of Cascade Flow Field Including Inlet Distortion and Rotating Stall," AFWAL-TR-87-2077, 1987.

[19]Briley, W. R. and McDonald, H., "Solution of the Multidimensional Compressible Navier-Stokes Equations by a Generalized Implicit Method," *Journal of Computational Physics,* Vol. 24, 1977, pp. 372–397.

[20]Briley, W. R. and McDonald, H., "On the Structure and Use of Linearized Block Implicit Schemes," *Journal of Computational Physics,* Vol. 34, No. 1, 1980, pp. 54–72.

[21]Shamroth, S. J., McDonald, H., and Briley, W. R., "Prediction of Cascade Flow Fields Using the Averaged Navier-Stokes Equations," *ASME Journal of Engineering for Gas Turbines and Power,* Vol. 106, No. 2, 1984, pp. 383–390.

[22]Weinberg, B. C., Yang, R.-J., McDonald, H., and Shamroth, S. J., "Calculation of Two- and Three-Dimensional Transonic Cascade Flow Fields Using the Navier-Stokes Equations," *Journal of Engineering for Gas Turbines and Power,* Vol. 108, No. 1, 1986, pp. 93–102.

[23]Rudy, D. H. and Bushnell, D. M., "A Rational Approach to the Use of Prandtl's Mixing Length in Free Turbulent Shear Flow Calculations," NASA SP-321, 1973, pp. 67–138.

[24]Ludwig, G. R., Nenni, J. P., and Arendt, R. H., "Investigation of Rotating Stall in Axial Flow Compressors and Development of a Prototype Rotating Stall Control System," AFAPL-TR-73-45, 1973.